A&A 403, 493–499 (2003)
DOI: 10.1051/0004-6361:20030245

Astronomy & Astrophysics

H-band observations of the Chandra Deep Field South⋆

E. Moy[1], P. Barmby[2], D. Rigopoulou[1], J.-S. Huang[2], S. P. Willner[2], and G. G. Fazio[2]

[1] Max-Planck-Institut für extraterrestrische Physik (MPE), Postfach 1312, Garching 85741, Germany
[2] Harvard-Smithsonian Center for Astrophysics, 60 Garden St., MS 65, Cambridge, MA 02138, USA

Received 7 November 2002 / Accepted 19 February 2003

Abstract. We report results of our *H*-band survey of the Chandra Deep Field South (CDFS). The observations, made with SofI on the NTT, cover 0.027 square degrees to $H < 20.5$ and 0.17 square degrees to $H < 19.8$ (50% completeness limits). In total, 4819 objects were detected, of which 80% are galaxies based on the SExtractor parameter "stellarity index" having a value less than 0.5. Our astrometric solutions are in good agreement with those of the Las Campanas Infrared Survey (LCIRS), the COMBO-17, and the ESO-EIS surveys. Our photometry compares satisfactorily with the LCIRS results as well as with GOODS data. Galaxy number counts are ∼50 000 galaxies per square degree at $H < 20.75$, in good agreement with those of LCIRS. The object catalog is published electronically at the CDS⋆⋆.

Key words. catalogs – surveys – infrared: general – galaxies: general – stars: general – cosmology: observations

1. Introduction

One of the many reasons for performing a deep survey is to study large-scale structure at high redshifts ($z \geq 1$) and to directly probe galaxy evolution from early epochs to the present day. Such studies allow us to trace the history of galaxy formation and evolution (Ellis 2001; Cohen et al. 2000) and to improve our understanding of the sources of the various components of the cosmic background (Totani et al. 2001; Madau & Pozzetti 2000). High redshift galaxies are often quite faint, and the use of spectroscopy to measure redshifts and other properties can be prohibitively expensive. The alternative way to estimate redshifts for large samples is to apply photometric techniques (Koo 1985; Fontana et al. 2000; Fernández-Soto et al. 1999; Le Borgne & Rocca-Volmerange 2002). This approach relies on the detection of typical SED features. Optical (*UBVRI*) data are able to detect the Balmer Break at 4000 Å up to $z \sim 1.3$, and the Lyman Break at 900 Å for $z \geq 3$ (Steidel et al. 1995). For $1.3 \leq z \leq 3$, the Balmer Break is redshifted beyond the *I* band and near infrared (NIR) data in the *J* and *H* bands are necessary to constrain the redshift with a high enough accuracy.

Currently, one of the best studied fields in the sky is the Chandra Deep Field South (CDF-S), located at J2000 coordinates $03^h32^m28^s$, $-27°48'30''$ (Giacconi et al. 2001). The CDF-S is a "blank" region of the southern sky chosen as the target for an extremely deep exposure with the *Chandra* X-ray Observatory. It has been the subject of observations with other space-based telescopes as well, including the Hubble Space Telescope (Schreier et al. 2001), as well as with numerous ground-based telescopes in the optical (Arnouts et al. 2001; Wolf et al. 2001), near-infrared (Saracco et al. 2001; Chen et al. 2002), and radio (Kellermann et al. 2000). Several sets of mid- and far-infrared observations with the upcoming Space Infrared Telescope Facility (SIRTF; Fanson et al. 1998) are planned, including Guaranteed Time Observations by the IRAC and MIPS instrument teams and Legacy program observations by the GOODS (Dickinson et al. 2003) and SWIRE (Franceschini et al. 2003) projects.

The ESO Imaging Survey (EIS) has performed the most extensive optical-NIR coverage of the CDF-S to date. It includes *UBVRI* observations covering 0.25 square degrees (Arnouts et al. 2001) and JK_s observations covering ∼400 square arcmin (Vandame et al. 2003). Filling the gap between these two filters is required by photometric redshift determination techniques, and necessitates observations of the CDFS in the *H* band. The COMBO-17 survey (Wolf et al. 2001) has imaged a $31.5' \times 30'$ field covering the CDF-S in 5 broad-band and 12 narrow-band filters, but with a wavelength coverage limited to the interval between 3650 and 9140 Å. The Las Campanas Infrared Survey (Firth et al. 2002; Chen et al. 2002) has recently performed *H*-band observations covering $25' \times 25'$ in the CDF-S, down to a 5 σ limiting magnitude of ∼20.5; however, their field is not centered on the *Chandra* observations.

The GOODS SIRTF Legacy team is observing a smaller ($10' \times 15'$) area of the CDF-S to a much greater depth than

Send offprint requests to: E. Moy,
e-mail: moy@discovery.saclay.cea.fr

⋆ Based on observations collected at the European Southern Observatory, Chile under programs 66.A-0451 and 68.A-0375.

⋆⋆ The whole catalog is only available in electronic form at the CDS via anonymous ftp to cdsarc.u-strasbg.fr (130.79.128.5) or via
http://cdsweb.u-strasbg.fr/cgi-bin/qcat?J/A+A/403/493

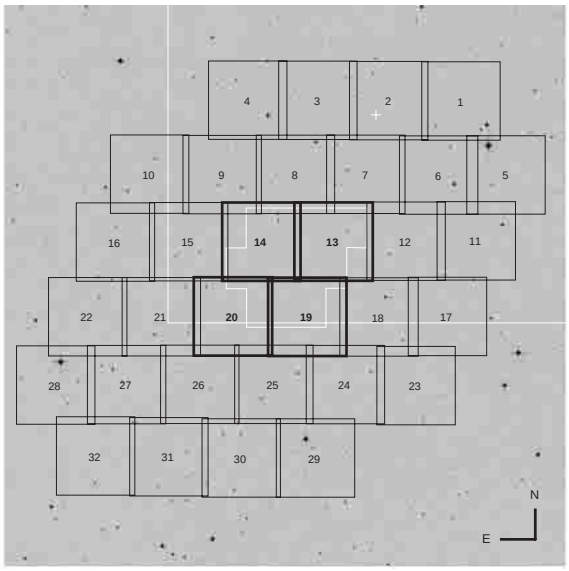

Fig. 1. The 32 SofI fields overlaid on a 35′ square Digitized Sky Survey image of the Chandra Deep Field South. Each SofI field is 4.9′ square; the deeper central fields are indicated by thicker outlines. The LCIRS survey area is the large white box centered on the cross in SofI field 2; the area covered by GOODS data release 0.5 is the white polygon within the central fields.

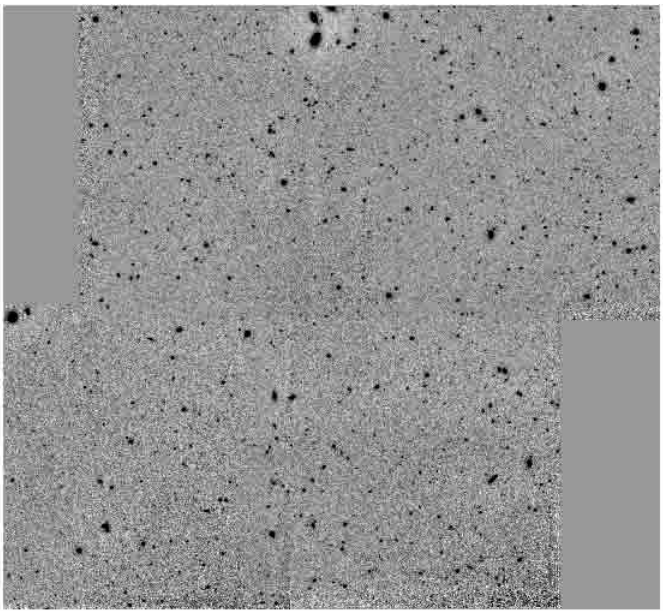

Fig. 2. Final *H*-band mosaic of the central ∼10 × 10 arcmin^2 of the CDFS (SOFI fields 13, 14, 15 and 19 in Fig. 1). North is up and East is left.

our observations, using ISAAC on the VLT. Their first data are available on the ESO web site.

We have conducted an *H*-band survey of the CDF-S, centered on the X-ray field, and encompassing the spatial coverage of the EIS observations as well as the future IRAC pointings. In the present paper we present the results of this survey. The observations and data reduction are described in Sect. 2; Sect. 3 presents the source extraction method and the resulting source lists. The survey performance is discussed in Sect. 4. Our conclusions are summarized in Sect. 5.

2. Observations and data reduction

2.1. Observations

We carried out the observations using the SofI near infrared imaging camera (Moorwood et al. 1998) installed on the ESO–NTT telescope at La Silla, during two observing runs: 15–18 November 2000 and 27–30 November 2001. The *H*-band filter of the SofI imaging mode is centered at 1.653 μm and is 0.297 μm wide. The SofI detector is a Hawaii HgCdTe 1024 × 1024 array. Sky conditions were photometric throughout the acquisition of the images with the seeing varying between 0.4–0.8″. We defined 32 4.9′ × 4.9′ fields covering the CDF-S area (see Fig. 1) and observed each of them in the "large field" configuration, with a scale of 0.288″ pixel^{-1}.

The observations were carried out using the "jitter" technique, one of the most efficient methods of sky acquisition with a minimum loss of observing time. The telescope is offset by small amounts around a central position. Offsets are generated randomly but are restricted within a square box. In our case the box width was 35″. A typical acquisition in jitter mode consisted of 60 1 min long frames, reaching a total integration time of 1 h. For the four central fields we repeated the sequence an additional three times, for a total of 4 h of integration time. Infrared standard stars from the Persson et al. (1998) list were observed every hour at similar airmasses to the science exposures.

2.2. Sky subtraction

Data reduction included the usual steps of flat-fielding (based on dome-flats) and bad pixel fixing, followed by a two-pass sky-subtraction. This method prevents bright objects from affecting the residual sky levels and thus the photometry of faint objects. The JITTER routine in ECLIPSE (Devillard 1999, 1997) was used to make the first-pass sky-subtraction and image registration. JITTER does not have an object-masking capability, so we used the DIMSUM package in IRAF[1] to co-add the first-pass images, derive an object mask from the co-added image, and redo the sky subtraction with objects masked. We then combined the final sky-subtracted images using JITTER (which is much faster than IRAF-based tools). A mosaic of the *H*-band images of the central fields is shown in Fig. 2.

2.3. Astrometry

We performed astrometric calibrations of the images using stars taken from the United States Naval Observatory (Monet 1998) and 2 Micron All Sky Survey (2MASS) databases. The astrometric solutions were computed using the tasks `ccmap` and `ccsetwcs` in the IRAF `imcoords` package. In order to check

[1] IRAF is distributed by the National Optical Astronomy Observatories, which are operated by the Association of Universities for Research in Astronomy, Inc., under cooperative agreement with the National Science Foundation.

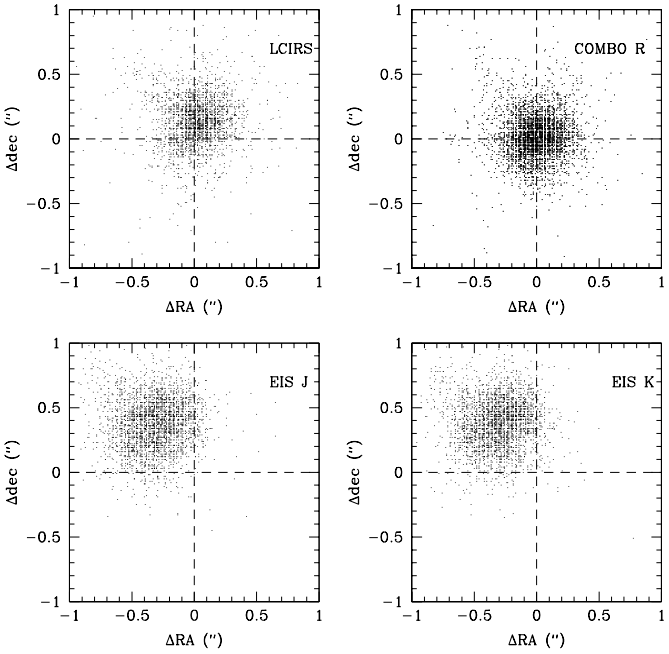

Fig. 3. Comparison between the coordinates of detections in common with the Las Campanas survey (top left), the *R*-band of the COMBO 17 survey (top right) and the *J* and K_s-bands of the EIS survey (bottom). All comparisons are in the sense (our coordinates) − (other survey coordinates).

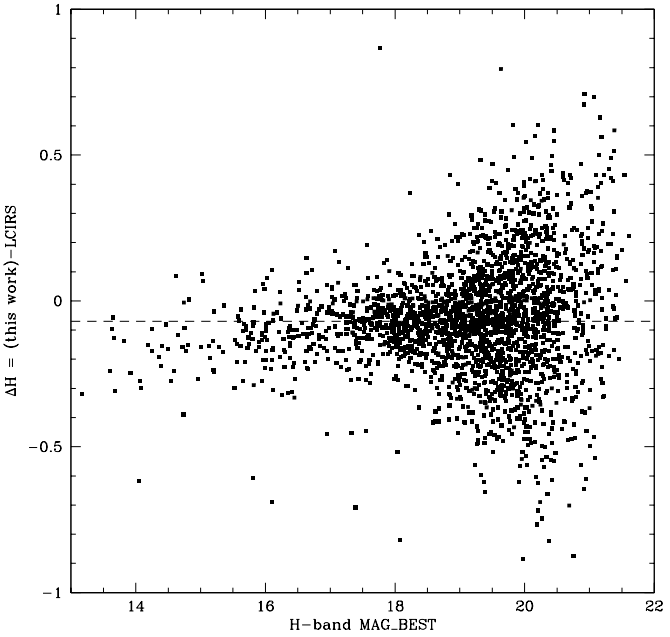

Fig. 4. Comparison of photometry between our data and that of LCIRS as a function of the *H*-band magnitude.

the accuracy of the astrometry our catalogs were compared with the source lists extracted from previous observations of the CDF-S. All comparisons were performed using J2000 coordinates. The relative offsets between the most likely counterparts of our *H*-band detections in the other source lists were computed, and the result is shown in Fig. 3. There is a negligible offset in right ascension and an offset of 0.15″ in declination between our data and the Las Campanas Infrared Survey (LCIRS) catalog. The rms in the difference is ≤0.24″ in both directions. The comparison is particularly good with the result of the COMBO-17 survey. The offsets are quite small (≤0.02″) in both directions, and the rms is only ∼0.2″. Arnouts et al. (2001) found an offset of ∼0.2″ in α and δ between the EIS and COMBO images. Not surprisingly, since COMBO astrometric calibrations are very similar to ours, we find a similar shift between our data and the EIS catalogs, ∼0.35″, with a rms of 0.2″.

2.4. Photometric calibration

We measured the instrumental magnitude of the standard stars in a 10-pixel (2.9″) radius aperture. The magnitude zeropoint of the corresponding exposure was computed as the difference between the instrumental and the cataloged *H*-band magnitudes. The zeropoints are compatible with other results listed on the NTT/SofI web page. Typical changes in the zeropoint over a night are ≤0.04 mag; since this includes real changes with the airmass, this value is probably an upper bound on the zeropoint error. For each CDF-S field (except the four central ones, see below), we took the average of the two values derived from the bracketing standard star observations as the zeropoint. For the co-added images of the four central fields, the median of the zeropoints computed for the individual exposures was adopted.

We tested our photometric calibrations by comparing the magnitudes measured by the LCIRS team and in the present work. For the comparison we used the "best" magnitude computed by Sextractor using the object profile. This quantity is a good estimate of the total magnitude of an object and should not depend on the seeing conditions during the observations. The result of the comparison is shown in Fig. 4. Our magnitudes are 0.065 mag brighter than those in LCIRS, with an rms of 0.22, for $14 \leq H \leq 19$. The cause of this difference is not known.

We also checked our measurements by doing photometry on CDF-S *H*-band included in the April 2002 (version 0.5) GOODS data release (Fig. 5). Altough the measured difference in magnitude is large for some individual galaxies, the result is quite satisfying, given the uncertainty on the GOODS zero points which are currently available. We find our magnitudes to be 0.014 mag fainter, on average, than those measured on the GOODS images, with an rms of 0.27.

3. Source list

Object detection was performed using version 2.2.2 of the SExtractor package (Bertin & Arnouts 1996). We performed one SExtractor run per field. Since the outermost parts of the images don't have a full 60-min exposure (due to the jitter technique), the signal-to-noise ratio strongly decreases in these areas. For most fields, this leads to many spurious detections close to the image borders, which were identified by eye and removed from individual catalogs. Thanks to a partial overlap (30″) between our pointings, the low S/N regions are

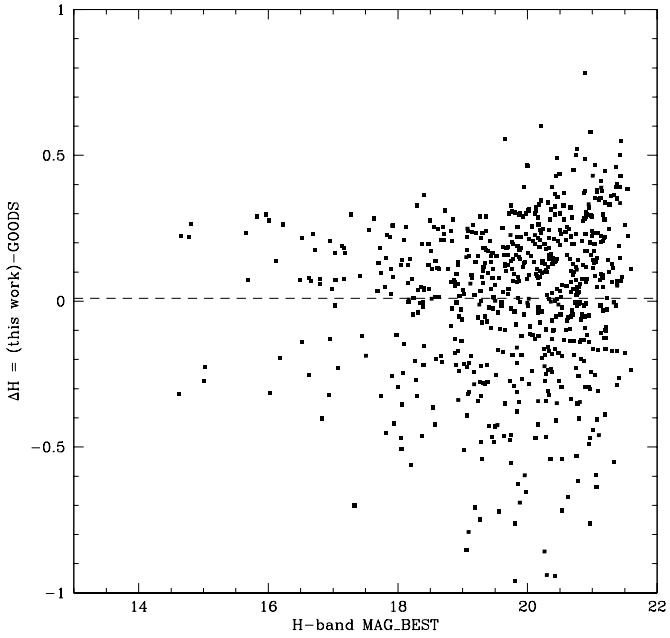

Fig. 5. Comparison of photometry between our data and that of GOODS as a function of the *H*-band magnitude.

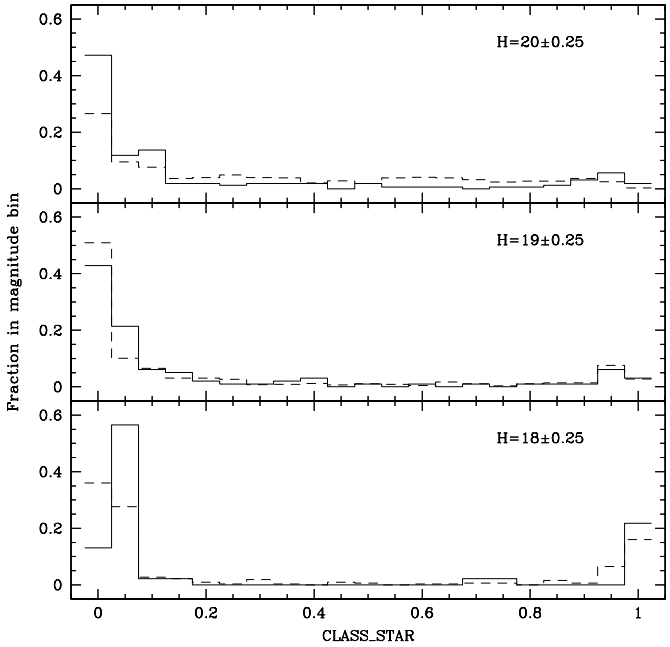

Fig. 6. Distribution of CLASS_STAR for objects in 3 different magnitude bins. The solid lines are for data in the inner fields, dashed lines for data in the outer fields.

covered to full depth in adjacent fields, except on the outside of the survey region.

For the extraction we used a 7×7 Gaussian filter with a FWHM of 3 pixels. Weight maps were computed from the image background to improve the quality of the source extraction by taking into account the image quality at each pixel. The SExtractor detection threshold was fixed to a conservative value of 3, and the minimum number of connected pixels above detection threshold to 5 for all fields. The initial catalogs were then cleaned of objects near saturated/hot pixels and objects where a reliable estimate of the flux was not feasible.

The final catalog contains 4819 objects, including 956 detections in the four deeper central fields. As an example, the first 40 entries of the final catalog are presented in Table 2. The following quantities are listed:

- Column 1: name.
- Column 2: field number.
- Columns 3 and 4: right ascension and declination (J2000).
- Columns 5–8: automatic and isophotal magnitudes and respective errors, as estimated by SExtractor.
- Columns 9–10: aperture magnitude (10 pixels, or 2.9″ diameter) and error.
- Column 11: SExtractor stellarity index.

4. Survey performance

4.1. Star-galaxy separation

Star/galaxy separation in deep observations is always challenging. Commonly used techniques are based on object morphology and/or colour properties (e.g. Gardner et al. 1996; Huang et al. 1997) when available. The SExtractor "stellarity index" (CLASS_STAR) is computed for a given object from the comparison of its luminosity profile with the natural "fuzziness" of the image, as estimated from the seeing FWHM. CLASS_STAR is equal to 0 for confirmed galaxies, and to 1 for confirmed stars. This quantity is known to be a robust galaxy identifier for objects brighter than a magnitude limit which depends on the observational conditions (e.g. Groenowegen et al. 2002).

In Fig. 6 we plot the distribution of the CLASS_STAR parameter for three different magnitude bins. For the brightest magnitude bin, the objects are concentrated at the two ends of the histogram, while in the faintest bin, the distribution is more uniform. Thus, we consider hereafter every object with CLASS_STAR ≤ 0.5 or fainter than $H = 19.75$ (outer fields) or $H = 20.25$ (inner fields) as a galaxy.

Our adopted value for the star/galaxy separation is a very conservative one. For instance Maiahara et al. (2000) have used a CLASS_STAR value of 0.8 (including small magnitude adjustments at the faint end) while the EIS classification was based on a CLASS_STAR parameter value of 0.9 (Arnouts et al. 2001). As is obvious from Fig. 6 our classification ensures that the galaxy sample does not suffer from possible contamination by misidentified stars.

4.2. Limiting magnitude

To estimate the completeness of our catalog, we used the standard procedure of trying to detect artificial objects inserted in the images. The IRAC "mkobject" task was used to simulate and add 40 stars and 40 galaxies to each field. The object magnitudes were distributed according to a shallow power law from 16.5 to 22.5 (17–23.5 for the central fields). The galaxy half-light radii were either 0.3″ (25% of the galaxies, chosen at random) or 0.7″; we found that this mix reproduced the distribution of (SExtractor parameters) FWHM vs. MAG_BEST found

Table 1. Table of 50% completeness limits for galaxies in the 32 individual SOFI fields.

Field #	Completeness limit
1	19.8
2	19.6
3	19.5
4	19.8
5	19.3
6	19.9
7	19.8
8	19.8
9	19.6
10	20.0
11	19.9
12	19.8
13	**20.7**
14	**20.7**
15	19.8
16	19.8
17	19.9
18	19.7
19	**20.3**
20	**20.4**
21	19.8
22	19.5
23	19.3
24	19.8
25	19.9
26	19.9
27	19.8
28	19.9
29	19.5
30	19.4
31	19.4
32	19.8

for our detected objects. The size of the PSF used to generate the stars and convolve with the galaxies was matched to the measured seeing in each field. Finally, we ran SExtractor on the resulting image, using exactly the same parameters as for real objects. The entire procedure was repeated 50 times for each field.

Figure 7 plots the histogram of our completeness estimation (i.e. number of artificial objects added/ number of artificial objects detected) for a few fields. We estimated the 50% completeness level for each image by spline-fitting the completeness histograms; for most of the outer fields, the 50% completeness level was $H = 19.8$. A few fields – generally those observed at higher airmass or in poorer seeing – had 50% completeness levels up to 0.5 mag brighter. The central fields were complete to fainter magnitudes: $H = 20.4$ for fields 19 and 20, and $H = 20.7$ for fields 13 and 14. The completeness limits are given for all fields in Table 1.

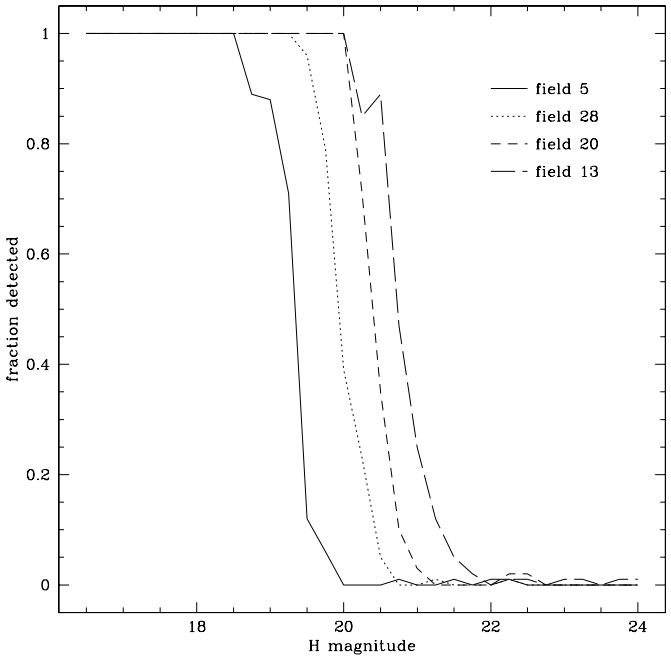

Fig. 7. Completeness data for fields 5, 28, 13 and 19. Fields 5 is the shallowest outer field, and field 28 is a typical outer field; fields 20 and 13 are the shallowest and deepest inner fields, respectively.

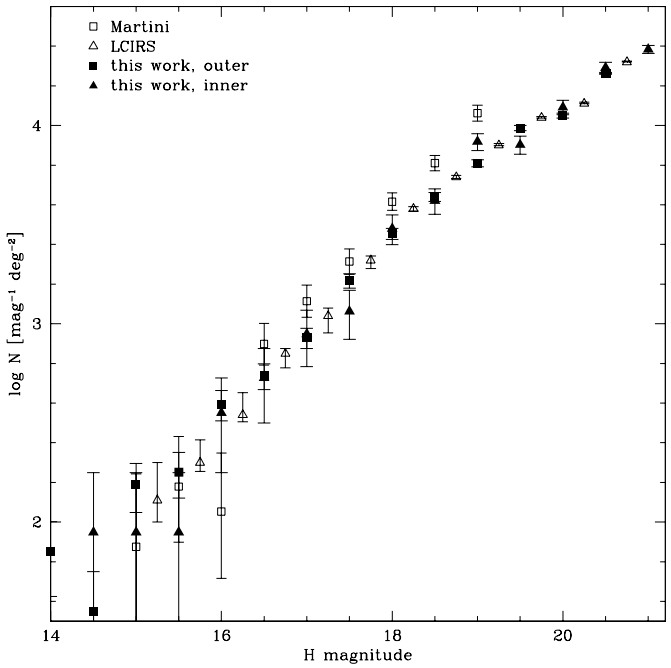

Fig. 8. Galaxy differential number counts for the outer and inner fields. Open symbols are data from Chen et al. (2002) and Martini (2001).

4.3. Number counts

We generated a completeness curve for each of the two regions as a sum of the completeness for the individual fields, weighted by the number of galaxies detected in each field. The galaxy counts from the combined catalogs are corrected for incompleteness using this curve, although in practice this is important only for the last 1 or 2 bins. Figure 8 shows the counts

Table 2. First 40 entries of the *H*-band source list. All magnitudes are in the Vega system.

Name	Field #	α (J2000)	δ (J2000)	$m_{\rm auto}$	$\delta m_{\rm auto}$	$m_{\rm iso}$	$\delta m_{\rm iso}$	$m_{\rm aper}$	$\delta m_{\rm aper}$	Class
CDFS−H-1	1	03:31:32.67	27:39:37.19	19.44	0.082	20.33	0.059	19.47	0.069	0.01
CDFS−H-2	1	03:31:35.81	27:39:29.39	19.72	0.083	20.76	0.069	19.75	0.077	0.00
CDFS−H-3	1	03:31:32.74	27:35:19.07	19.31	0.053	19.65	0.038	19.29	0.045	0.00
CDFS−H-4	1	03:31:35.02	27:35:04.61	19.37	0.051	19.54	0.034	19.38	0.053	0.16
CDFS−H-5	1	03:31:41.52	27:35:05.13	19.78	0.068	20.02	0.043	19.73	0.076	0.60
CDFS−H-6	1	03:31:29.99	27:35:22.20	19.58	0.068	20.02	0.042	19.59	0.058	0.00
CDFS−H-7	1	03:31:31.95	27:35:22.88	17.86	0.019	17.99	0.013	18.02	0.014	0.02
CDFS−H-8	1	03:31:28.27	27:35:24.90	17.81	0.013	17.86	0.010	17.84	0.012	0.47
CDFS−H-9	1	03:31:27.16	27:35:27.22	13.19	0.000	13.17	0.000	13.25	0.000	0.98
CDFS−H-10	1	03:31:40.40	27:35:24.21	19.99	0.084	20.58	0.055	19.94	0.085	0.27
CDFS−H-11	1	03:31:29.58	27:35:29.29	16.35	0.004	16.37	0.003	16.39	0.003	0.98
CDFS−H-12	1	03:31:25.50	27:35:29.82	19.64	0.091	20.89	0.082	19.65	0.104	0.72
CDFS−H-13	1	03:31:36.00	27:35:34.12	15.15	0.001	15.14	0.001	15.17	0.001	1.00
CDFS−H-14	1	03:31:32.33	27:35:35.10	19.61	0.064	19.95	0.038	19.64	0.061	0.02
CDFS−H-15	1	03:31:37.93	27:35:41.06	18.25	0.023	18.39	0.017	18.35	0.019	0.02
CDFS−H-16	1	03:31:40.07	27:35:44.24	18.09	0.026	18.39	0.019	18.35	0.020	0.01
CDFS−H-17	1	03:31:29.16	27:35:49.17	19.61	0.078	20.89	0.072	19.67	0.062	0.00
CDFS−H-18	1	03:31:40.11	27:35:51.96	15.97	0.003	15.97	0.003	15.99	0.002	0.98
CDFS−H-19	1	03:31:36.93	27:35:53.85	17.99	0.015	18.05	0.012	18.00	0.014	0.99
CDFS−H-20	1	03:31:41.53	27:35:55.89	19.75	0.074	20.54	0.057	19.73	0.070	0.00
CDFS−H-21	1	03:31:27.31	27:35:57.41	19.93	0.085	21.52	0.095	19.98	0.084	0.00
CDFS−H-22	1	03:31:29.34	27:36:01.93	19.20	0.062	20.34	0.053	19.49	0.052	0.00
CDFS−H-23	1	03:31:26.57	27:36:03.81	19.32	0.068	20.07	0.047	19.48	0.061	0.06
CDFS−H-24	1	03:31:27.36	27:36:06.38	19.25	0.067	20.42	0.057	19.51	0.055	0.00
CDFS−H-25	1	03:31:35.87	27:36:10.69	14.96	0.001	14.96	0.001	14.99	0.001	1.00
CDFS−H-26	1	03:31:31.18	27:36:12.70	18.88	0.048	19.40	0.033	19.10	0.038	0.00
CDFS−H-27	1	03:31:25.98	27:36:18.18	19.55	0.082	20.54	0.066	19.61	0.079	0.00
CDFS−H-28	1	03:31:39.31	27:36:17.86	20.51	0.101	21.31	0.074	20.41	0.128	0.60
CDFS−H-29	1	03:31:28.53	27:36:19.57	18.63	0.028	18.76	0.020	18.66	0.024	0.02
CDFS−H-30	1	03:31:32.00	27:36:22.13	20.45	0.070	20.86	0.056	20.53	0.139	0.69
CDFS−H-31	1	03:31:32.23	27:36:23.73	19.33	0.052	19.66	0.032	19.36	0.048	0.01
CDFS−H-32	1	03:31:29.29	27:36:24.05	18.72	0.038	19.05	0.025	18.85	0.029	0.00
CDFS−H-33	1	03:31:27.76	27:36:25.23	20.29	0.088	21.14	0.067	20.25	0.106	0.21
CDFS−H-34	1	03:31:36.60	27:36:26.34	17.67	0.016	17.83	0.012	17.81	0.012	0.03
CDFS−H-35	1	03:31:45.09	27:36:25.25	19.38	0.044	19.74	0.036	19.42	0.053	0.05
CDFS−H-36	1	03:31:46.20	27:36:26.22	19.59	0.057	19.97	0.044	19.57	0.062	0.00
CDFS−H-37	1	03:31:44.05	27:36:26.97	18.61	0.034	18.86	0.023	18.70	0.028	0.02
CDFS−H-38	1	03:31:28.79	27:36:29.49	19.81	0.073	21.41	0.084	19.87	0.074	0.00
CDFS−H-39	1	03:31:40.31	27:36:40.08	19.01	0.042	19.20	0.027	19.07	0.038	0.18
CDFS−H-40	1	03:31:44.32	27:36:40.36	19.06	0.050	19.40	0.031	19.09	0.039	0.01

for the outer and inner fields, together with comparison data from other groups. Our galaxy counts match those of Chen et al. (2002) extremely well; the counts of Martini (2001) are somewhat higher, and Chen et al. (2002) attribute this to an incorrect magnitude correction on the part of Martini (2001). The number counts in different magnitude bins between $H = 14$ and $H = 21$ are given in Table 3.

5. Summary

We have performed an *H*-band survey of the Chandra Deep Field South covering 0.17 square degrees down to a limiting magnitude of $H_{\rm Vega} \sim 20$. The resulting catalog includes more than 3800 galaxies. We find that our astrometry and photometry are in generally good agreement with other surveys in the region, and our derived galaxy number counts agree well with results from other surveys.

The present work fills the gap between the *J* and *K* band data in the EIS database of the CDF-S, allowing the determination of accurate photometric redshifts for a large range of *z*. When combined with already existing optical data, the present data will primarily be used to filter out low-*z* sources in preparation for the upcoming mid-infrared SIRTF surveys on the CDFS.

Table 3. Total number of objets n, number of galaxies n_g and galaxy number counts N (in $mag^{-1}\,deg^{-2}$, corrected for incompleteness) as a function of magnitude.

	outer			inner		
H	n	n_g	N	n	n_g	N
14.0	78	6	71 ± 29	1	0	0
14.5	28	3	36 ± 21	2	1	89 ± 89
15.0	33	13	154 ± 43	5	1	89 ± 89
15.5	47	15	178 ± 46	3	1	89 ± 89
16.0	74	33	392 ± 68	12	4	355 ± 178
16.5	89	46	546 ± 81	13	6	533 ± 218
17.0	122	70	848 ± 99	18	10	888 ± 281
17.5	210	136	1648 ± 138	17	13	1155 ± 320
18.0	325	237	2843 ± 183	46	34	3021 ± 518
18.5	449	360	4363 ± 225	60	47	4176 ± 609
19.0	642	516	6451 ± 270	98	84	8292 ± 814
19.5	829	654	9709 ± 304	124	90	7996 ± 843
20.0	708	708	11211 ± 316	161	135	12365 ± 1032
20.5	216	216	18323 ± 175	194	194	19586 ± 1237
21.0				169	169	24216 ± 1155

Acknowledgements. We would like to thank ou referee, Patrick McCarthy, for his useful suggestions and comments. EM acknowledges support of the EU TMR Network "Probing the Origin of the Extragalactic Background Radiation" (HPRN-CT-2000-00138). This publication makes use of data products from the Two Micron All Sky Survey, which is a joint project of the University of Massachusetts and the Infrared Processing and Analysis Center/California Institute of Technology, funded by the National Aeronautics and Space Administration and the National Science Foundation.

References

Arnouts, S., Vandame, B., Benoist, C., et al. 2001, A&A, 379, 740
Bertin, E., & Arnouts, S. 1996, A&AS, 117, 393
Cohen, J. G., Hogg, D., Blandford, R., et al. 2000, ApJ, 539, 29
Chen, H.-W., Mc Carthy, P. J., Marzke, R. O., et al. 2002, ApJ, 570, 54
Devillard, N. 1997, The Messenger, 87, 19
Devillard, N. 1999, in Astronomical Data Analysis Software and Systems VII, ed. D. M. Mehringer, R. L. Plante, & D. A. Roberts, 333
Dickinson, M., Giavalisco, M., & the GOODS team 2003, in The Mass of Galaxies at Low and High Redshift, Proc. of the ESO Workshop held in Venice, Italy, 24-26 October 2001, 34 ed. R. Bender, & A. Renzini [astro-ph/0204213]
Ellis, R. S. 2001, PASP, 113, 515
Fanson, J., Fazio, G., Houck, J., et al. 1998, in ed. P. Y. Bely, & J. B. Breckinridge, Proc. SPIE 3356, Space Telescopes and Instruments, SPIE (Bellingham, WA), 478
Fernández-Soto, A., Lanzetta, K. M., & Yahill, A. 1999, ApJ, 513, 34
Firth, A. E., Somerville, R. S., Mc Mahon, R. G., et al. 2002, MNRAS, 332, 617
Fontana, A., D'Odorico, S., Poli, F., et al. 2000, AJ, 120, 2206
Franceschini, A., Lonsdale, C., and The Swire Co-Investigator Team 2003, in The Mass of Galaxies at Low and High Redshift, Proc. of the ESO Workshop held in Venice, Italy, 24-26 October 2001, p. 338
Gardner, J. P., Sharples, R. M., Carrasco, B. E., & Frenk, C. S. 1996, MNRAS, 282, L1
Giacconi, R., Rosati, P., Tozzi, P., et al. 2001, ApJ, 551, 624
Groenewegen, M. A. T., Girardi, L., Hatziminaoglou, E., et al. 2002, A&A, 392, 741
Kellermann, K. I., Fomalont, E. B., Rosati, P., et al. 2000, Am. Astron. Soc. Meet., 197, 9002
Koo, D. C. 1985, AJ, 90, 418
Le Borgne, D., & Rocca-Volmerange, B. 2002, A&A, 386, 446
Madau, P., & Pozzetti, L. 2000, MNRAS, 312, 9
Martini, P. 2001, AJ, 121, 598
Monet, D. 1998, BAAS, 30, 1427
Moorwood, A., Cuby, J.-G., & Lidman, C. 1998, The Messenger, 91, 9
Persson, S. E., Murphy, D. C., Krzeminski, W., Roth, M., & Rieke, M. J. 1998, AJ, 116, 2475
Saracco, P., Giallongo, E., Cristiani, S., et al. 2001, A&A, 375, 1
Schreier, E. J., Koekemoer, A. M., Grogin, N. A., et al. 2001, ApJ, 560, 127
Steidel, C. C., Pettini, M., & Hamilton, D. 1995, AJ, 110, 2519
Totani, T., Yoshii, Y., Iwamuro, F., Maihara, T., & Motohara, K. 2001, ApJ, 550, L137
Vandame, B., Olsen, L. F., Jørgensen, H. E., et al. 2003, A&A, submitted [astro-ph/0102300]
Wolf, C., Dye, S., Kleinheinrich, M., et al. 2001, A&A, 377, 442